WP20–JRA1: Lidar and sunphotometer – Improved instruments, integrated observations and combined algorithms

Deliverable D20.2: Report on evaluation of Raman lidar techniques for daytime extinction measurements

Objectives

Task 1 of WP20 aims at the improvement of daytime capabilities of lidar instruments, in particular for the measurement of aerosol extinction profiles in the UV (355 nm) and visible wavelength range (532 nm). So far, most of the EARLINET multi-wavelength Raman lidar observations are performed at night, because Raman signals are weak compared to daylight background. Different techniques have been developed to improve Raman lidar daytime capabilities in the past years. The techniques are based on small-bandwidth emitter and receiver systems and on a small receiver field of view to suppress the daylight background. They have been successfully tested and implemented in a few systems which are already in operational use within EARLINET.

Within WP20, an in-depth investigation of the optical and mechanical design requirements of Raman lidar instruments shall be carried out, with the goal to obtain optimum performance under daylight conditions and with focus on easy-to-implement and robust solutions. The results shall be used to give recommendations for the respective improvement of existing instruments within the network. In this report, we review the state-of-the-art and provide a list of references.

Requirements

Raman lidar observations at daytime require a number of methodical and instrumental efforts, which are briefly discussed in the following.

1) Optimization of molecular signal intensity

The Rayleigh-Raman spectrum of nitrogen and oxygen, which are used as reference gases in the atmosphere, is shown in Fig. 1 for the emission wavelength of 355 nm. Conventional Raman lidar systems applied in EARLINET use vibration-rotation Raman transitions of nitrogen (first Stokes band, at 387 nm in Fig. 1) to detect a molecular reference signal of the atmosphere, from which particle extinction coefficient profiles are retrieved. In this case, the separation of elastic and inelastic backscatter signals is not problematic and can easily be realized with dichroic beamsplitters and interference filters centered at the wavelengths of interest. However, the scattering cross section of the vibration-rotation Raman band is about 1500 times smaller than the one of the Rayleigh line. Therefore, signals are weak and strongly disturbed by daylight background. An improvement of signal intensity is possible when rotational Raman transitions are used instead. The scattering cross section of the rotational Raman band of nitrogen and oxygen is about 40 times higher than the one of the first Stokes band of nitrogen.

When rotational Raman signals are to be measured, great care must be taken in the separation of the Raman return from the elastically backscattered light in order to avoid any cross-talk, since the rotational Raman lines are located close to the exciting laser wavelength. Usually, not the entire rotational Raman spectrum will be measured and thus not the full intensity of the band will be used for several reasons:

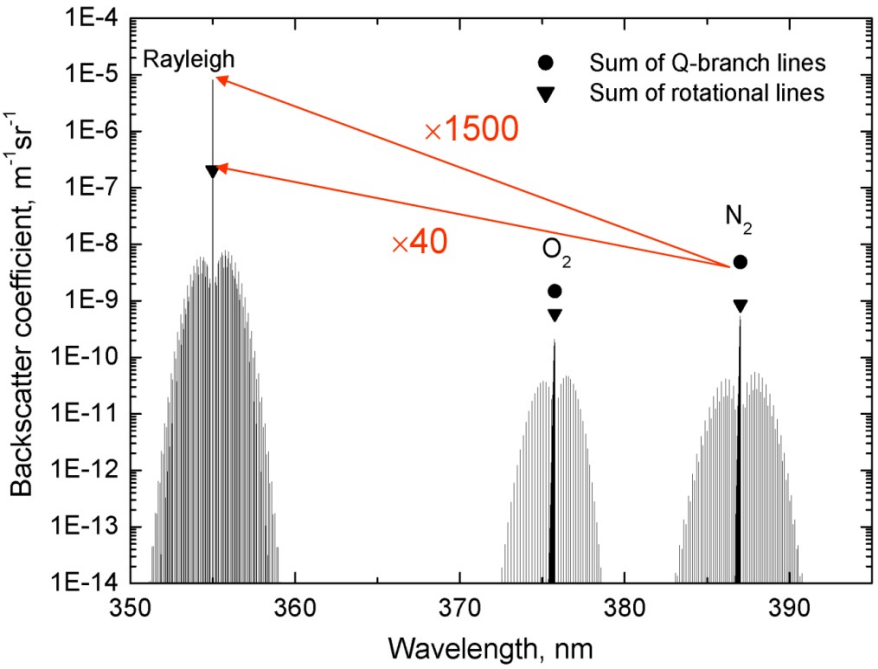

Fig. 1: Rayleigh-Raman spectrum of nitrogen and oxygen for an emission wavelength of 355 nm and surface conditions.

- Spectral separation of lines located closest to the laser emission wavelength is difficult.
- The width of the rotational Raman band contradicts the requirement of narrow-bandwidth detection in order to suppress daylight background (see below). Thus, only the most intense lines should be selected.
- The intensity distribution within the band depends on temperature. By selecting two (or more) parts of the spectrum with different temperature dependence one can determine atmospheric temperature profiles. Up to now, this has been the primary goal of rotational Raman lidar developments and the option should be kept even when extinction measurements are envisaged.

The temperature dependence of the signal intensity when only parts of the rotational Raman spectrum are measured must be minimized or appropriately corrected before extinction profiles can be retrieved from rotational Raman signals.

2) Narrow-bandwidth detection

The contribution of sky background to a lidar signal decreases linearly with decreasing receiver bandwidth. Therefore, narrow-bandwidth detection is required for Raman daytime applications. Narrow-bandwidth detection can be realized in different ways by applying either interference-filter or grating spectrometer techniques. Technical implementations are discussed below. Narrow-bandwidth detection requires a stable laser emission frequency and a sufficiently narrow spectral distribution of the emitted light as well. Depending on the laser source, the implementation of an injection seeder may become necessary.

In general, narrow-bandwidth solutions show a higher sensitivity with respect to atmospheric temperature, angular distribution of light rays in the receiver, and mechanical/adjustment stability compared to conventional Raman lidar setups. Higher complexity of the optical setups in conjunction with higher costs is the consequence. Therefore, optimization efforts are strongly required.

3) Small receiver field of view

A small receiver field of view (FOV) is an indispensable requirement for daytime Raman applications, because the sky background contribution to a lidar signal increases quadratically with the FOV. However, a small receiver FOV prohibits the detection of signals in the near range of the telescope. Thus, it contradicts combined lidar and sun photometer retrievals, which require complete lidar aerosol profiles throughout the atmosphere and which are in the focus of WP20. Here we need solutions based on observations with two or more telescopes that can cover different height ranges. Furthermore, a small FOV requires very good system stability in order to guarantee that the laser beam always remains in the FOV. An automatic control of the laser pointing stability during the measurement is advisable. Again, optimization efforts in view of system complexity, stability, and costs are strongly required.

Techniques

Two specific techniques for rotational Raman lidar observations have been implemented. The first one is based on the application of narrow-band interference filters, the second one uses the grating technology. A brief review of both methods is provided in the following.

1) Rotational Raman lidar techniques based on narrow-band interference filters

Rotational Raman lidars based on the interference-filter technique have been described for a laser wavelength of 532 nm first [Vaughan et al., 1993; Nedeljkovic et al., 1993; Behrendt and Reichardt, 2000]. The application of the technique at 355 nm has been demonstrated by Di Girolamo et al. [2004] and Radlach et al. [2008]. Daytime temperature profiling with this technique was shown by Behrendt et al. [2002], Di Girolamo et al. [2004], and Radlach et al. [2008].

The filters to select parts of the rotational Raman band usually have a bandwidth of 0.2 to 0.6 nm in the UV and 0.5 to 1.5 nm in the visible. A very efficient design at 532 nm has been proposed by Behrendt and Reichardt [2000]. As shown in Fig. 2, the filters are mounted sequentially at small angles of incidence. Light that is transmitted as well as light that is reflected by the filters is detected. Therefore, high detection efficiency is reached. Furthermore, the center wavelengths of the filters are adjustable via the angle of incidence. High suppression of the elastic backscatter signal in the rotational Raman detection channels has been demonstrated with this setup. Radlach et al. [2008] applied the same principle at 355 nm.

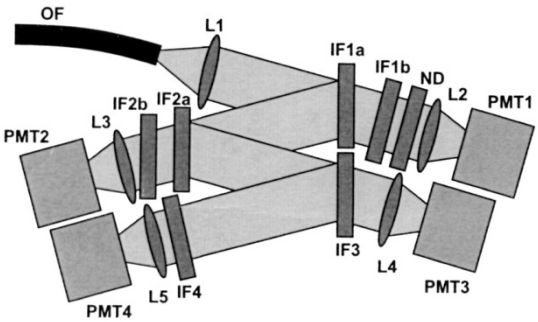

Fig. 2: Sequential interference filter setup for the measurement of rotational Raman signals (with PMT2 and PMT3), elastic backscattering (with PMT1) and N_2 vibration-rotation Raman scattering (with PMT4). OF, optical fiber; L1–L5, lenses; IF1a–IF4, interference filters; ND, neutral density attenuator; PMT1–PMT4, photomultiplier tubes. Figure taken from Behrendt and Reichardt [2000].

A new approach was proposed by Reichardt et al. [2012] and implemented in the Raman lidar RAMSES (Raman lidar for Atmospheric Moisture SEnSing) of the German Meteorological Service in Lindenberg, Germany. It makes use of the polarization properties of rotational Raman lines to separate two

temperature-dependent signals. The interference filters are employed under normal incidence in this case. When linearly polarized laser light is emitted, the backscattered rotational Raman radiation has a fixed depolarization ratio of 75%. Therefore, the backscatter signal can be split into a co-polar and cross-polar part in the receiver, which gives two signals of similar strength. The use of two linearly polarized signals has some further advantage regarding the suppression of cross-talk from elastically scattered light. Details are explained in Reichardt et al. [2012].

A somewhat simplified setup, based on the same principle and using the same interference filters and polarization beam splitter cube as in RAMSES, has been implemented in the EARLINET Raman lidar MARTHA (Multiwavelength Atmospheric Raman lidar for Temperature, Humidity, and Aerosol profiling) at Leipzig. A part of the far-range receiver setup of MARTHA showing three out of the 14 detection channels is presented in Fig. 3. The rotational Raman channels are equipped with interference filters with center wavelengths of 355.4 and 356.3 nm for a laser emission wavelength of 354.7 nm. The filter bandwidths are 0.2 and 0.6 nm, respectively. The 355.4-nm channel (so-called cold channel, because the intensity in this channel increases with decreasing temperature; the 356.3-nm channel is called the warm channel because of the opposite temperature sensitivity) is supplied with an additional edge filter, which assures sufficient suppression of the elastically backscattered light. The edge filter curve must be shifted to the appropriate position by tuning the angle of incidence. This procedure is strongly polarization dependent and thus supported by the predefinition of the polarization state with the polarizing beam splitter cube.

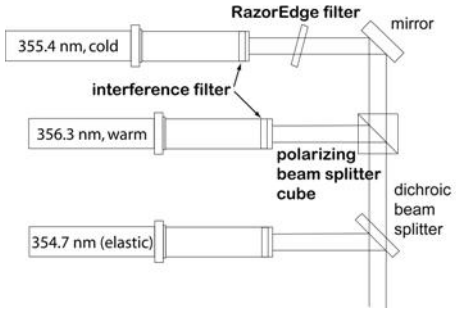

Fig. 3: Part of the MARTHA receiver setup showing the rotational Raman channels and the elastic-backscatter channel for the emission wavelength of 354.7 nm.

The optical setup of both systems RAMSES and MARTHA has been designed with professional ray-tracing software, and detailed sensitivity studies have been performed. Design and optimization studies in ACTRIS WP20, Task 1 can also build on this expertise.

2) Rotational Raman lidar techniques based on gratings

Use of diffraction-grating polychromators for filtering pure rotational Raman spectra (PRRS) of atmospheric nitrogen and oxygen molecules has a long history which started in the early 1980s [e.g., Arshinov et al., 1983]. The technique has been tested and successfully implemented in the visible spectral range, ultraviolet, and solar-blind region [e.g., Mattis et al., 2002; Serikov et al., 2010]. The basic principle of the grating filtering technique is illustrated in Fig. 4 with a sketch of a fiber-coupled double-grating polychromator.

In the presented configuration, the diffraction angle is dependent on wavelength, and therefore PRRS and the elastic component of light are split in the diffracted beam. Spectral filtering is achieved then as a spatial filtering, with the central wavelength and spectral width of filtered light defined by the position of the output fiber along the dispersion axis and the fiber core diameter, see Fig. 5a. Four output fibers are used in the first chamber of the polychromator to isolate lines with negative and positive temperature sensitivity in both the Stokes and anti-Stokes branch of PRRS. Another output fiber picks up the elastic component of the spectrum.

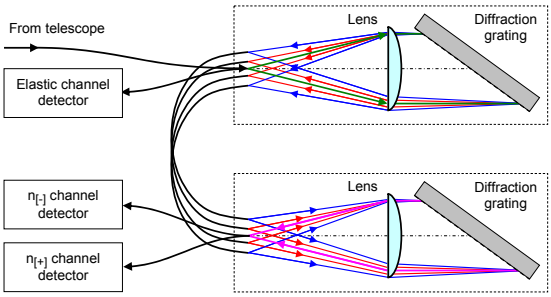

Fig. 4: Example of a diffraction-grating polychromator. Footnotes [+] and [-] indicate two channels with positive and negative temperature sensitivity.

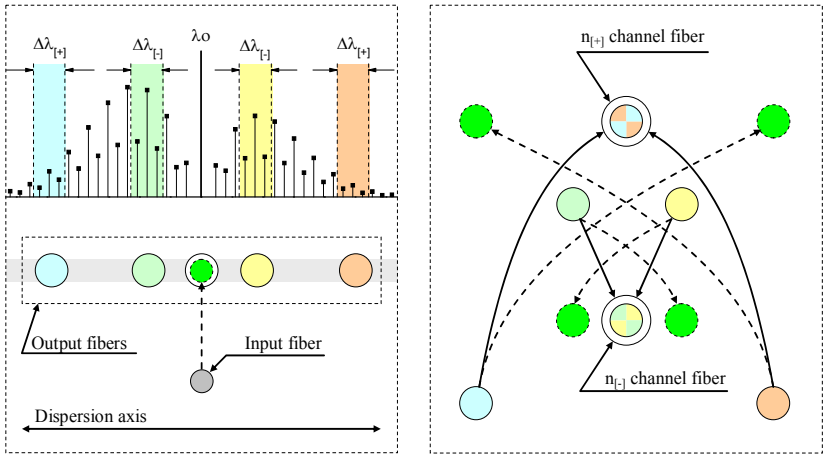

Fig. 5: Fiber arrangement in the lens focal plane of the first (a) and second (b) chamber of the polychromator. Dashed and solid arrows indicate the position of the fiber image for elastic and inelastic light, respectively. The spatial distribution of PRRS of nitrogen in diffracted light is schematically shown in panel (a).

Detecting returns in Stokes and anti-Stokes branches increases the signal intensity by about a factor of two compared to the interference-filter approach where only one branch is used. Coupling the output fibers of the first chamber to the second one, while keeping the same fiber position along the dispersion axis, allows so-called subtraction of dispersion, i.e. the image of each fiber for inelastic light has the same position along the dispersion axis, see Fig. 5b. In this configuration Stokes and anti-Stokes components of PRRS with identical temperature dependence are combined in one output channel. The image of each input fiber for elastic light is displaced along the dispersion axis from the inelastic image, see Fig. 5b, explaining an additional elastic-light suppression. With this double-stage filtering the total cross-talk between elastic and Raman channels is minimized to about eight orders of magnitude. To give an estimate: when measuring air temperature in clouds with this pure rotational Raman lidar technique, the suppression is sufficient to minimize the cross-talk-induced bias to less than 0.1 K.

The grating filtering technique is easy to extend for a multi-telescope setup, which is required to cover an extended operational range with narrow-field-of-view detection. Fig. 6, for instance, represents a fiber assembly for the four-telescope configuration implemented in the EARLINET Raman lidar of the Max Planck Institute (MPI), Hamburg, Germany. With this fiber bundle only one polychromator, as shown in Fig. 4, is used for four telescopes. A compact fiber package (fiber bundle size does not exceed 12 mm $\times$ 12 mm) supports enhanced alignment stability. The alignment procedure does not differ from that for a one-telescope configuration and does not take longer: when the polychromator is aligned for one telescope, it is automatically aligned for the other three. Cost efficiency of such extension is another obvious advantage.

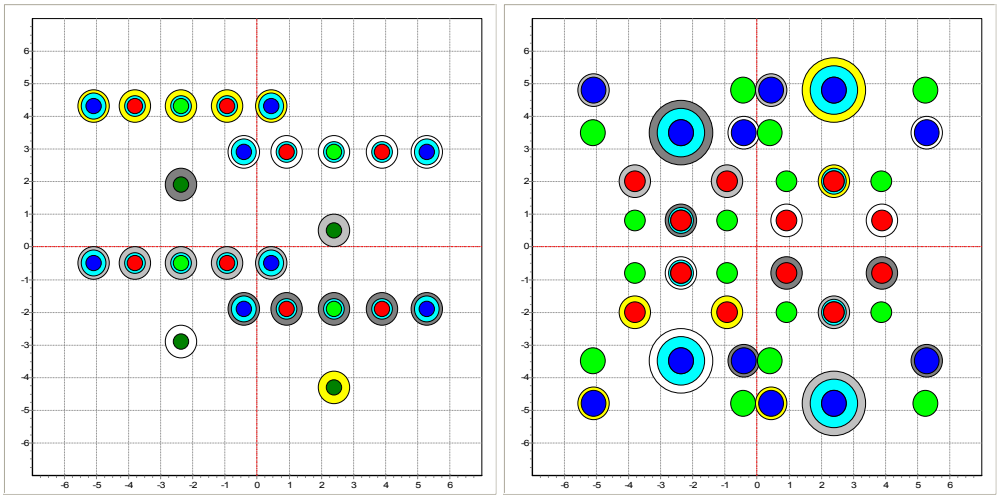

(a) (b)

Fig.6. Fiber assembly of first (a) and second (b) polychromator chamber for the four-telescope configuration of the MPI Raman lidar. Different colors of fiber cladding (white, light gray, dark gray, yellow) mark four different input channels.

The daytime capability of the diffraction-grating filtering technique in multi-telescope configuration is tested with the MPI Raman lidar permanently deployed on Barbados Island (13.16 N, 59.43 W) since April 2010. Some of results are presented on the project web-page at http://barbados.zmaw.de/lidarql/dp2011/.

References

Yu. F. Arshinov, S. M. Bobrovnikov, V. E. Zuev, and V. M. Mitev, 1983: Atmospheric temperature measurements using a pure rotational Raman lidar, Appl.Opt. 22, 2984–2990.

A. Behrendt and J. Reichardt, 2000: Atmospheric temperature profiling in the presence of clouds with a pure rotational Raman lidar by use of an interference-filter-based polychromator, Appl. Opt. 39, 1372–1378.

A. Behrendt, T. Nakamura, M. Onishi, R. Baumgart, and T. Tsuda, 2002: Combined Raman lidar for the measurement of atmospheric temperature, water vapor, particle extinction coefficient, and particle backscatter coefficient, Appl. Opt. 41, 7657–7666.

P. Di Girolamo, R. Marchese, D. N. Whiteman, and B. B. Demoz, 2004: Rotational Raman Lidar measurements of atmospheric temperature in the UV, Geophys. Res. Lett. 31, L01106, doi:10.1029/2003GL018342.

I. Mattis, A. Ansmann, D. Althausen, V. Jaenisch, U. Wandinger, D. Müller, Y. F. Arshinov, S. M. Bobrovnikov, and I. B. Serikov, 2002: Relative-humidity profiling in the troposphere with a Raman lidar, Appl. Opt. 41, 6451–6462.

D. Nedeljkovic, A. Hauchecorne, and M. L. Chanin, 1993: Rotational Raman lidar to measure the atmospheric temperature from the ground to 30 km, IEEE Trans. Geosci. Remote Sens. 31, 90–101.

M. Radlach, A. Behrendt, and V. Wulfmeyer, 2008: Scanning rotational Raman lidar at 355 nm for the measurement of tropospheric temperature fields, Atmos. Chem. Phys. 8, 159–169.

J. Reichardt, U. Wandinger, V. Klein, I. Mattis, B. Hilber, and R. Begbie, 2012: RAMSES: The German Meteorological Service autonomous Raman lidar for water vapor, temperature, aerosol, and cloud measurements, submitted to Appl. Opt.

I. Serikov and S. Bobrovnikov, 2010: Atmospheric temperature profiling with pure rotational Raman lidars, in: L. Fiorani, V. Mitev *Series: Optoelectronic Material and Devices Volume 7: Recent Advances in Atmospheric Science*. Bucharest: INOE, 149–216.

G. Vaughan, D. P. Wareing, S. J. Pepler, L. Thomas, and V. Mitev, 1993: Atmospheric temperature measurements made by rotational Raman scattering, Appl. Opt. 32, 2758–2764.